Highlights

Ab initio study of the adsorption of O, O_2, H_2O and H_2O_2 on UO_2 surfaces using DFT+U and non-collinear magnetism

Ine Arts, Rolando Saniz, Gianguido Baldinozzi, Gregory Leinders, Marc Verwerft, Dirk Lamoen

- Full non-collinear approach that accounts for spin-orbit coupling and $3k$ (transverse) magnetic order with the PBE+U functional.
- Assessment of electronic structure and oxidation state of the surface uranium with and without adsorption.
- Detailed study of H_2O_2 adsorption on UO_2 surfaces.
- Planar magnetic order at the UO_2 surface.

Ab initio study of the adsorption of O, O_2, H_2O and H_2O_2 on UO_2 surfaces using DFT+U and non-collinear magnetism

Ine Arts[a], Rolando Saniz[b], Gianguido Baldinozzi[c], Gregory Leinders[d], Marc Verwerft[d], Dirk Lamoen[a]

[a]*EMAT & NANOlab Center of Excellence, Department of Physics, University of Antwerp, B-2020, Antwerp, Belgium*
[b]*CMT & NANOlab Center of Excellence, Department of Physics, University of Antwerp, B-2020, Antwerp, Belgium*
[c]*Université Paris-Saclay, CentraleSupélec, CNRS, SPMS, F-91190, Gif-sur-Yvette, France*
[d]*Belgian Nuclear Research Centre (SCK CEN), Institute for Nuclear Energy Technology, B-2400, Mol, Belgium*

Abstract

In order to model correctly the corrosion of spent nuclear fuel under disposal conditions, it is important to understand its behavior in the presence of oxidants. To advance in this direction, we consider the oxidation of UO_2. We investigate computationally the adsorption of various species on its three most stable surfaces: (111), (110), and (100), with emphasis on incorporating a full non-collinear PBE+U approach. Various species, namely O, O_2, H_2O and H_2O_2 are considered due to their relevance for the oxidation of UO_2. The dissociation energy and an estimate for the dissociation barrier for O_2 were obtained, using the preferred adsorption configurations of O and O_2. The adsorption configurations for H_2O in our study compare well with previous studies that used collinear approximations, both in terms of relative stability of configurations and bond lengths. Differences in adsorption energies were found, which may be important for reaction kinetics. Dissociative reactions in which the water molecule splits in hydrogen and hydroxyl occur only on one of the three surfaces. The hydrogen further reacts with a surface oxygen to also form a hydroxyl group. Not surprisingly, we find that H_2O_2 binds more strongly to the three surfaces than water (lower formation energy), and similar to H_2O adsorption, dissociative reactions may occur. The dissociated hydrogen reacts with a surface oxygen to form a hydroxyl group and the hydroperoxyl molecule binds with a surface uranium. Our study, which includes a detailed study of electron transfer, magnetic structure and the preferred adsorption configurations, gives insight into the uranium oxidation states and the influence of surface geometry on adsorption. The findings contribute to a more comprehensive understanding of the early stages of UO_2 oxidation.

Keywords: UO_2, surface oxidation, DFT+U, non-collinear magnetism, spent nuclear fuel

1. Introduction

Alike many countries, Belgium considers the direct disposal of spent nuclear fuel in a deep geological disposal as a safe long term option. Today's reference layout involves packing of SNF assemblies in multilayered steel/concrete containers ("Supercontainer concept") which are then loaded in disposal galleries carved in stable geological clay layers [63, 30, 29]. These containers are engineered to withstand ingress of groundwater for several millennia, but ultimately, engineered barriers will degrade, as will the metallic cladding tubes holding the nuclear fuel. After several thousand years, the spent fuel will thus come in contact with water. Fission-generated nuclides (fission products, actinides and activation products) might then gradually dissolve and may start migrating. The corrosion process of the UO_2 matrix itself is the rate-determining factor in the release rate of many nuclides (in particular the actinides) during this stage.

At its earliest stage, low-temperature oxidation of UO_2 in dry air involves the molecular or dissociative adsorption (chemisorption) of oxygen (O_2) gas onto the UO_2 surface [51, 38, 35]. The heat of chemisorption has been reported as -230 kJ/mol, declining to -20 kJ/mol in later stages [20]. During the oxidation process, oxygen ions become incorporated as interstitials into the fluorite structure of UO_2, which can effectively accommodate disorder, creating hyperstoichiometric UO_{2+x} [31]. The excess oxygen aggregates with intrinsic Frenkel pair defects prevalent in near-stoichiometric UO_2, which can be either isolated or start to form aggregates, depending on the departure from stoichiometry [1, 2]. Subjected to lower temperatures (below 250 °C), bulk stoichiometry is limited to $x = 0.03$, because the solubility of oxygen is reduced with decreasing temperature [7, 35].

Further oxidation then results in formation of higher oxides near the reaction interface [7, 58]. Below 100 °C, the diffusion of oxygen ions becomes exceedingly slow, as it is no longer thermally activated, effectively limiting any oxidation to the surface [14]. (Note that this is for a system with no extrinsic doping, which changes the oxidation [41].) This regime is called field-assisted oxidation. In this regime oxygen diffusion is facilitated by a potential difference, due to the chemisorption of oxygen, which leads to the transfer of electrons to the surface. This electric field enables the transport of oxygen ions through the oxide layer but only to a certain depth within the material [11, 22].

When exposed to water, the formation of higher-valence uranium compounds, such as schoepite or metaschoepite, is observed, potentially due to a dissolution-precipitation mechanism [12]. The initial stage of UO_2 surface oxidation in moist environments involves the adsorption of water onto the surface. This process begins with a precursor state of physical adsorption of water molecules (physisorption) and is followed by a combination of partial dissociation (resulting in H^+ and OH^-) and complete dissociation (resulting in $2H^+$ and O^-) to form chemisorbed products [13, 62]. At temperatures below 100 °C, water was found to be more strongly oxidizing, whereas at higher temperatures, oxygen becomes more effective in oxidizing UO_2 [14]. This oxidation predominantly occurs at the surface of the sample,

making the microstructure and surface area critical factors in influencing this process [12].

Instead of relying solely on experimental approaches, researchers have turned to atomistic *ab initio* calculations, which are, however, mainly limited to investigating the very initial stages of interfacial interactions, specifically the process of adsorption. A significant body of research has been dedicated to the theoretical study of adsorption onto UO_2 surfaces, with most of these studies utilizing the GGA+U methodology within the DFT framework.
The focus of these investigations has primarily been on the adsorption of water molecules, and all three primary UO_2 surfaces have been subjected to extensive scrutiny. On the (111) surface, these studies have revealed that both molecular and dissociative adsorption of water exhibit nearly equivalent energies. However, on the (110) and (100) surfaces, a clear preference for dissociative adsorption has been observed [65, 66, 9, 60]. This has been studied as a function of water coverage [8, 50, 37, 59]. Additionally, when examining reduced UO_2 surfaces where oxygen vacancies are present, there is a consistent preference for dissociative water adsorption across all surfaces [61, 66]. Pegg and coworkers [46, 44] furthermore focused their computational work on adsorption of atomic hydrogen and H_2.

With the exception of the more recent research on hydrogen adsorption, the studies mentioned previously do not include non-collinear magnetism and spin-orbit coupling (SOC) into their models. One could argue that the magnetic structure is irrelevant at oxidation conditions, but non-magnetic calculations are no suitable alternative for modeling the paramagnetic phase of UO_2. The omission of non-collinear magnetism is primarily due to the computational complexity. Instead, many of these studies have simplified their models by using collinear $1k$ anti-ferromagnetic (AFM) magnetism or even assuming a ferromagnetic arrangement [9, 9, 65, 50]. However, it was indicated that the use of collinear magnetism does not allow for the reorientation of magnetic moments in the surface layer [45].

In the present study, we focus on modeling adsorption on the three most stable, low-indexed UO_2 surfaces: (111), (110), and (100). Importantly, this investigation incorporates a full non-collinear approach, accounting for SOC and $3k$ (transverse) magnetic order. We consider the adsorption behavior of various species, namely atomic oxygen (O), oxygen molecules (O_2), water (H_2O), and hydrogen peroxide (H_2O_2). The study of H_2 [44, 46], O_2 and H_2O_2 is motivated by radiolysis of water under repository conditions [36, 55, 40, 49, 23]. By considering non-collinear magnetism and spin-orbit coupling, this research aims to provide a more accurate and comprehensive understanding of the adsorption processes on these UO_2 surfaces.

2. Computational methodology

2.1. Electronic structure

The electronic structure calculations were performed using the *Vienna ab initio simulation package* (VASP) code [27], which uses projector-augmented-wave pseudopotentials to describe core-valence interactions [28]. The valence electrons that are explicitly considered

are U: $6s^2 6p^6 5f^3 6d^1 7s^2$, O: $2s^2 2p^4$ and H: $1s^1$, they are expanded in a plane wave basis set with a cutoff energy of 600 eV. The exchange-correlation functional used is the Perdew-Burke-Ernzerhof (PBE) generalized gradient approximation (GGA) [48].

For actinides, due to strongly correlated f-electrons, standard GGA's do not perform well [10, 16, 33, 52]. They induce an erroneous delocalized state because the self-interaction is not cancelled out correctly. To account for this, we employed the PBE+U method. Here a screened on-site Coulomb interaction is introduced to penalize partial filling of the uranium f-states. The specific formalism used is that of Dudarev [17], as implemented in VASP. The value for the Hubbard U parameter is the same for all uranium atoms ($U_{\text{eff}} = U - J = 4.0$ eV), which is the typically accepted value in literature as it has been estimated from experiments [6, 54, 26] and shown to perform well in calculations [8, 47, 17, 21, 5, 57, 68]. Although there have been efforts to calculate these parameters using cRPA, which yields a considerably higher value of $U_{\text{eff}} = 5.7 - 0.4$ eV [3], the Hubbard parameter has also been tuned to produce the correct band gap and lattice parameter, which leads to a lower value of $U_{\text{eff}} = 3.35$ eV [43].

Self-consistent calculations are performed until the energy difference reaches 10^{-6} eV. Forces are converged within 10 meV/Å. The calculations include spin-orbit coupling and take the non-collinear $3k$ (transverse) magnetic ground state [18] into account.

Though DFT+U calculations are known to converge to local minima, no occupation control method was used in this work. The OMC method was required for the efficient exploration of the energy of the microstates of the f-manifold [15]. SOC lifts the degeneracy of these states, reducing the need for occupation control. Moreover, the breaking of symmetry by non-collinear magnetism, Jahn-Teller distortion, and the presence of an interface are all contributing factors that diminish the possibility of converging to spurious minima [4, 67].

2.2. Surface model

The three most stable UO_2 ((111), (110) and (100)) surfaces are modeled using the symmetric slab model. This ensures that there is no net dipole present [56]. The surface slab is created by cleaving from bulk, with a vacuum layer of at least 18 Å to avoid interactions along the surface normal (chosen as the z-direction) and slab thickness of minimum 15 Å, so that the middle layer is bulk-like. For the UO_2 (111)-surface this entails 7 O-U-O layers (28 formula units), with a cell size of 53.4 Å^2 × 41 Å, for the (110)-surface this is 13 UO_2 layers (26 formula units), with a cell size of 43.5 Å^2 × 44 Å and the (100)-surface has 7 U-O_2 layers (28 formula units), with a cell size of 61.6 Å^2 × 41 Å. This last surface would give rise to a net electric dipole due to the alternately charged O_2 and U layers. In order to avoid this, the surface was stabilized by using an O-terminated surface instead of the full O_2 monolayer and then the slab was symmetrized. This is as if half of the oxygen atoms were transferred from the top O_2 layer to the bottom U layer. It is described by [17] and supported experimentally [42].

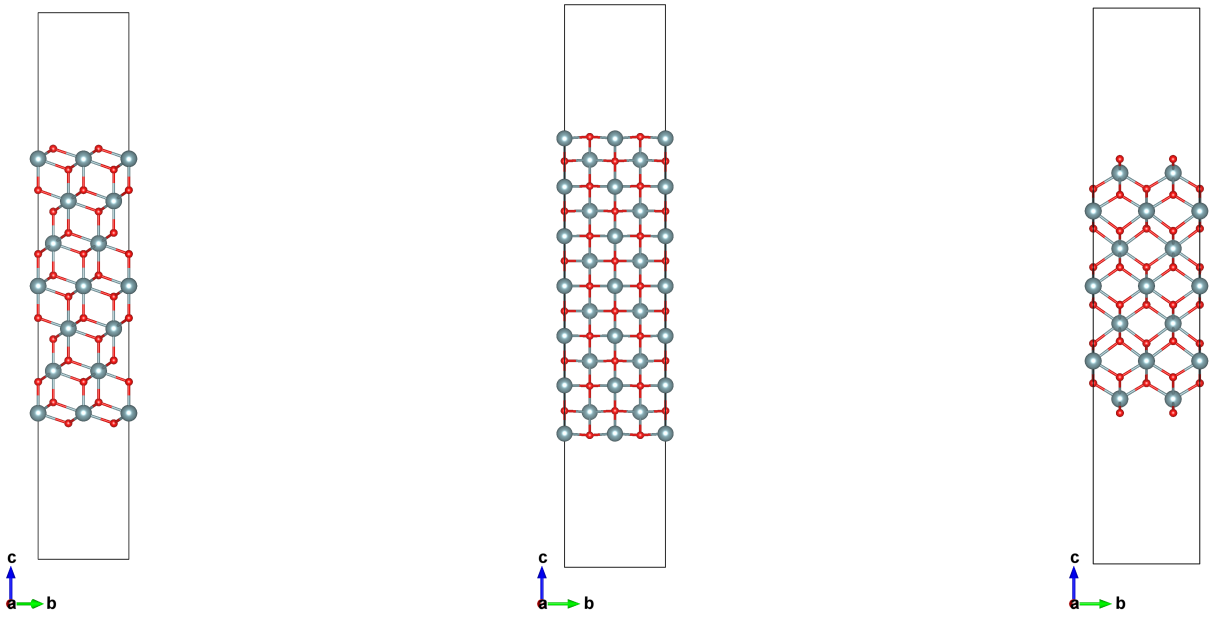

(a) (111) (b) (110) (c) (100)

Figure 1: The investigated UO_2 surface models ((111), (110) and (100) respectively) with relaxed atomic positions. The width of the vacuum is at least 18 Å.

All three surface slab models use a Monkhorst-Pack k-point grid of 3x3x1 k-points. Van der Waals interactions are included in the adsorption calculations, using the method of Grimme, as implemented in the VASP code [24]. The starting magnetic moments are those of bulk UO_2. The modulus of the initialized moments is 1.7 μ_B, projected along four directions and rotated to match the new relative orientations of the UO_2 lattice with respect to each Cartesian coordinate frame. They are given in Table S2 in the supporting information.

Adsorption is simulated by performing a full atomic relaxation of both the adsorbate and the slab, with the exception of the middle layer. For each adsorbate and surface 4 different initial adsorption sites at a distance of 1 Å from the surface are used as initial configuration. These adsorption sites are shown in Fig. 2 and can be referred to as U (a), O (b), bridge (c) or hollow (d) sites. The adsorption energy is defined as follows:

$$E_{ads}(X) = E_{slab}(X) - (E_{slab} - N_X\mu_X) \quad (1)$$

Where $E_{slab}(X)$ and E_{slab} are the total DFT energies of the slab model, including relaxation, with and without adsorbed molecule X, N_X the number of these molecules adsorbed (always even using the symmetric slab model) and μ_X the chemical potential of the molecule. The latter is approximated by the total energy of the isolated molecule.

The surface energy is a formation energy per surface area (the factor 2 is due to the sym-

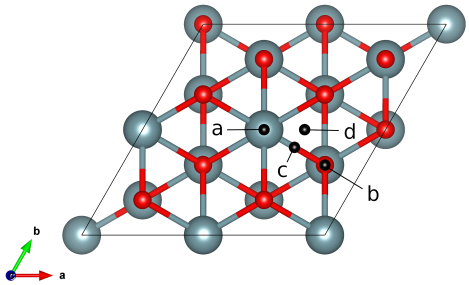

Figure 2: Investigated adsorption sites on the UO_2 (111)-surface (only the topmost layer is shown). U (a), O (b), bridge (c) and hollow (d) sites.

metric slab model as two surfaces are present):

$$E_{surf} = \frac{1}{2A}\left(E_{slab} - NE_{bulk}\right) \tag{2}$$

Bader charge analysis is used to derive atomic charges of the individual atoms from the quantum mechanical charge density. The partitions over which is integrated are defined by zero-flux surfaces in the charge density [25].

3. Results

3.1. Bulk UO_2

As a reference, calculations on bulk UO_2 are discussed first. These calculations were performed in the same way as described above, using PBE+U, magnetic order and spin-orbit coupling and with an MP k-point grid of 6×6×6 k-points. Table 1 gives an overview of the different magnetic orders $1k$ to $3k$ both transverse and longitudinal. These configurations are defined in [47].

Computationally, the experimental $3k$ transverse magnetic order is not found as the ground state ($1k$ transverse has the lowest energy by 11 meV/unit cell, Table 1); a shortcoming of the functional approximation. However, only the $3k$ transverse order is compatible with the experimentally observed $Pa\bar{3}$ symmetry where the oxygen atoms are displaced in the (111) directions and furthermore, collinear anti-ferromagnetism breaks the cubic symmetry. The calculated oxygen displacement is 0.0043 Å, factor 3 smaller than measured with neutron diffraction (0.014 Å) [19].

The calculated lattice constant is 5.546 Å, 1.37 % larger than experiment [34] (x-ray diffraction), but within range of other *ab initio* studies. U-O bond lengths are due to the oxygen displacement between 2.395 and 2.403 Å. The calculated band gap is 2.71 eV and the total magnetic moment at a U site is 1.68 μ_B, compared to experimental values of 2-2.5 eV [53, 39] and 1.74 μ_B [18], respectively. The density-of-states (DOS) is given in Fig. 3a. For consistency, the surface models that are used in this work are based on the DFT-optimized

magnetic order	ΔE **(eV/unit cell)**	**spacegroup**	**O displacement (Å)**
1k long.	0.013	I4/mmm	/
1k transv.	0	I4/mmm	/
2k long.	0.010	Fm$\bar{3}$m	/
2k transv.	0.009	Cmce	0.0055
3k long.	0.007	Fm$\bar{3}$m	/
3k transv.	0.011	Pa$\bar{3}$	0.0043
3k *transv.*	*experimental*	*Pa$\bar{3}$*	*0.014*

Table 1: PBE+U [48, 17] with SOC - Relative stability of antiferromagnetic orders in UO_2 with respect to the 1k transverse order.

magnetic order	ΔE **(eV/unit cell)**	**spacegroup**	**O displacement (Å)**
1k	0	I4/mmm	/
2k	3.156	I4/mmm	/
3k	3.926	Fm$\bar{3}$m	/

Table 2: PBE+U [48, 17] without SOC - Relative stability of antiferromagnetic orders in UO_2 with respect to the 1k transverse order. Transverse and longitudinal configurations are degenerate without SOC.

bulk structure.

In this work we do account for noncollinear magnetism and spin-orbit interactions, for two reasons. The first was highlighted by Pegg and coworkers [45]: collinear approximations cannot reorient the magnetic moments relative to both the surface plane and the bulk-like layers. Therefore, simulations would compare different magnetic structures along the different surfaces. Secondly, though it does not affect surface energies, it does affect the electronic structure (which can be seen in Fig. 3a for the bands around -20 to -15 eV) and thus could affect bonding and adsorption, which is the main interest of this study.

3.2. Pristine surface

Surface energies calculated for the (111), (110) and (100) are 0.72 J/m^2, 1.08 J/m^2 and 1.52 J/m^2, respectively. Comparing this to values reported in the literature review of Wang et al. [64] (an overview can be found in Table S1 in the supporting information), surface energies are, as mentioned, unaffected by the inclusion of spin-orbit interactions and noncollinear magnetism.

3.2.1. (111) surface

The relaxation of the (111) surface leads to a slight contraction of the interlayer distance of the outer two successive uranium layers of 0.04 Å. The U-O bond length decreases by 0.05 Å for the top U and O monolayer. Uranium atoms of the first layer have a coordination of 7 (8 in bulk UO_2), while the oxygen of the first monolayer has 3 (4 in bulk UO_2). The magnitude of the spin moments shows a small deviation for the outer layer of U atoms (1.61 μ_B, compared to 1.56 μ_B for the inner layers, 1.54 μ_B in bulk), yet there is no significant difference in Bader charges between the uranium atoms.

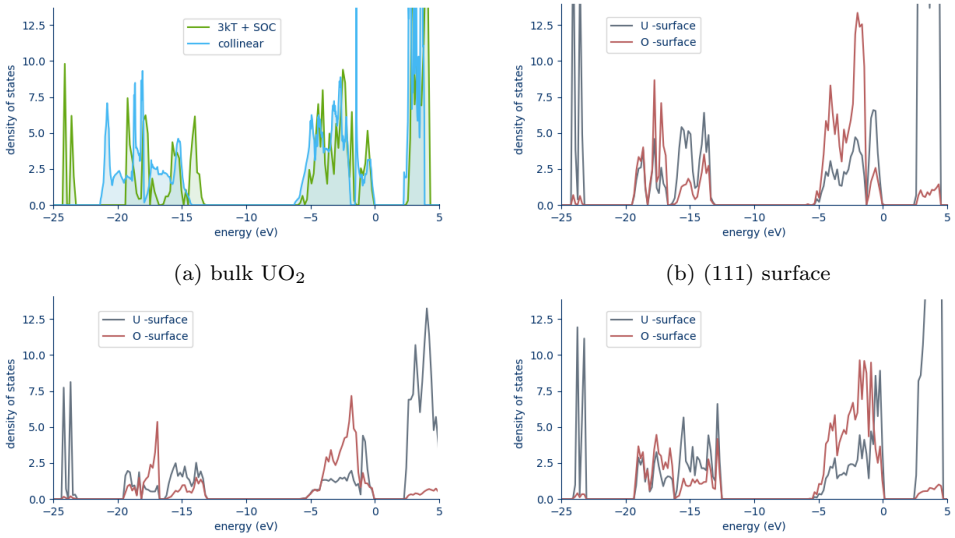

(a) bulk UO_2 (b) (111) surface

(c) (110) surface (d) (100) surface

Figure 3: DOS for UO_2. a) bulk UO_2: shows the difference between collinear AFM (blue) calculation and non-collinear $3k$ transverse AFM with SOC (green). b), c) and d) are the DOS for the (111), (110) and (100) respectively, for which only the partial contributions of the surface atoms are shown: uranium in grey and oxygen in red.

3.2.2. (110) surface

More noticeably in the (110) surface, a contraction of interlayer distance of 0.3 Å between the first two layers, with an increase of 0.1 Å in the next layer, has been found. There is a decrease of 0.04 Å for the U-O bond lengths within the first monolayer, of 0.15 Å for U_{layer1}-O_{layer2} and of 0.07 Å for U_{layer2}-O_{layer1}, due to the interlayer distances. The coordination of U and O of the outer layer is 6 and 3, respectively. The U atoms of the outer layer have a spin moment of 1.67 μ_B, while the other U atoms carry 1.56 μ_B (1.54 μ_B in bulk). Bader analysis indicates electron transfer from O to U, within the outer layer, of 0.08 per U atom.

3.2.3. (100) surface

Unlike the other surfaces, the relaxation of the (100) surface leads to an increase of 0.03 Å for the interlayer distance of the outer 2 uranium layers. The U-O distances of the outer two monolayers decreased by 0.20 Å, while the oxygen in the second oxygen layer shifts up and down according to the pattern of the vacancies in the topmost O layer, thus there is both an increase and decrease (by 0.15 Å) for these U-O bond lengths. The outer uranium layers have a coordination of 6 and the oxygen of the outer monolayer has a coordination of 2. Similar to the (110) surface, the U atoms in the first layer have a spin moment of 1.67 μ_B (1.56 μ_B in bulk layers and 1.54 μ_B in bulk) and Bader charge transfer of 0.07 electrons to U.

For all three surfaces we see that the magnitude of the spin moment is the same as the bulk value for all uranium atoms that are not in the surface layer. The small deviation of spin moment at the surface of the order of 0.10 μ_B (and small electron transfer to these

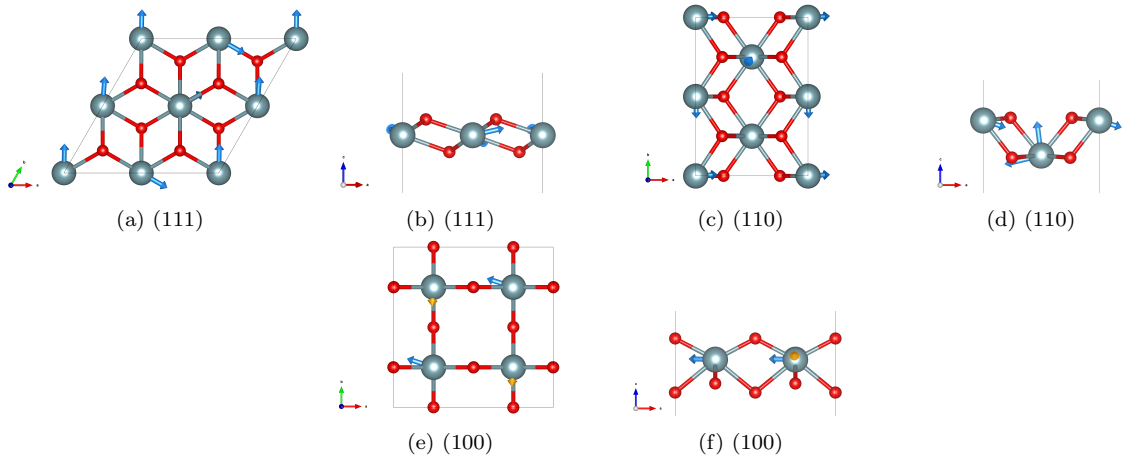

(a) (111) (b) (111) (c) (110) (d) (110)

(e) (100) (f) (100)

Figure 4: Converged magnetic moments (sum of spin and orbital part) for the three UO_2 surface models. a), c) and e) give a view perpendicular to the surface, b), d) and f) offer a side view along the a or b axis. The yellow arrows in e) and f) have been scaled up for visibility.

atoms) is explained by the decrease in coordination and U-O bond lengths at the surface. The orbital contribution to the magnetic moment is always larger than the spin part, consistent with previous calculations on uranium compounds. It is in the same direction, but with a different sign than the spin contribution, with a small angular deviation for some atoms at the surface of less than 3°, 1.5° and 5° for the (111), (110) and (100) surface respectively. Though the magnitude of the orbital part of the magnetic moments varies for different atoms in the slab model, bulk values are recovered in the middle layers. This is shown in Fig. S1 in the supporting information.

The DOS of only the surface layer has been given in Fig. 3. The magnetic configuration at the surface has been analysed. In the topmost surface layer, the total magnetic moments (sum of spin and orbital contribution) are realigned towards the plane of the surface, as demonstrated in Fig. 4 and similar to [45]. The values are given in Tables S4, S5 and S6 in the supporting information.

3.3. Adsorption

Inequivalent final configurations have been identified, based on the geometry of the relaxed calculations, and grouped together with equivalent configurations on other surfaces. They will be categorized under chemi- or physisorption, based on following properties: Bader analysis, atomic distances and DOS.

3.3.1. O radical adsorption

In all adsorption calculations the oxygen atom (or radical) creates an ionic bond with the surface, either to a uranium or an oxygen atom after relaxation. A summary is given in Table 3. In the lowest energy configuration the chemisorbed atom will increase the coordination of the U atom to resemble more that of bulk UO_2 (Fig. 5a, 5c and 5e). For the (100) surface this is a bond to two surface U atoms (Fig. 5e). Depending on the surface geometry the U

configuration	$\|OU_1\|$ (Å)	$\|OO_1\|$ (Å)	E_{ads} (eV)	e^- transfer
(111) surface				
U-site chemisorption (5a)	1.82	/	-0.19	0.87
O-site chemisorption (5b)	2.49	1.48	0.34	0.60
(110) surface				
U-site chemisorption (5c)	1.81	/	-1.06	0.86
O-site chemisorption (5d)	2.27	1.48	0.24	0.62
(100) surface				
U-site chemisorption (5e)	1.95, 2.33	/	-1.80	1.06
O-site chemisorption (5f)	2.42	1.51	-0.24	0.64

Table 3: Summary of the adsorption of the oxygen radical. In the first column the final configurations is described, followed by the relevant bond lengths, adsorption energies and Bader charge transfer from the surface to the adsorbate. U_1 and O_1 are labeled in Figure 5.

coordination will increase from 7 to 8 for the (111) or from 6 to 7 for both (110) and (100). The spin moment of the surface U atom decreases from 1.61 and 1.67 to 0 μ_B for the (111) and (110) surfaces respectively (Table. S6 in SI), indicating oxidation state +VI, while the two U atoms of the (100) surface have a decreased spin moment of 0.8 μ_B compared to 1.67 μ_B in the pristine surface, leading to oxidation state +V [33]. The U-O bond length is 1.8 Å, which is 25% shorter than in bulk UO_2. Adsorption to the U site is the lowest energy configuration and is exothermic on all 3 surfaces. In the DOS (Fig. 5a, 5c and 5e) clear hybridization between the oxygen atom and the surface uranium is visible as a broadening of the oxygen states at -4 eV and -18 eV. The oxygen contribution of the DOS behaves similarly to the DOS of oxygen in bulk UO_2.
In the case of atomic oxygen binding to a surface oxygen atom, peroxide (O_2^{2-}) is formed on the surface (Fig. 5b, 5d and 5f). This is indicated by the O-O bond length of 1.5 Å and electron transfer from the surface to the adsorbed atom (Table S7 in SI). This is exothermic only on the least-stable (100)-surface. In the DOS (Fig. 5b, 5d and 5f) one can again see hybridization in the form of broadening of the peaks. They now overlap with states of the oxygen atom of the surface indicating their bond.

3.3.2. O_2 molecule adsorption

Two cases are found for the O_2 molecule: physisorption and chemisorption, see Fig. 6. On all three surfaces a physisorbed case is found. Its adsorption energy lies between -0.05 and -0.24 eV, as indicated in Table 4. No charge transfer is found and the O-O bond length has not changed. The distance to the nearest surface atom is larger than the sum of the covalent radii. The molecule has a high spin state (1.5 μ_B, Table S8 in SI). In the DOS, states belonging to the O_2 adsorbate are sharp and narrow i.e. molecule-like and there is no hybridization with states of the surface, as seen in Fig. 6a, 6b and 6d.
On the two higher energy surfaces ((110) and (100)) chemisorption of O_2 is also found (Fig. 6c and 6e). Compared to physisorption, it is characterized by a stronger bonding and a shorter bond length. For this case we find a more negative adsorption energy and electron transfer to the molecule. The O_2 bond length has increased from 1.24 Å to 1.33 Å, indicative of superoxide (O_2^-) due to the transferred electron from the surface uranium atom

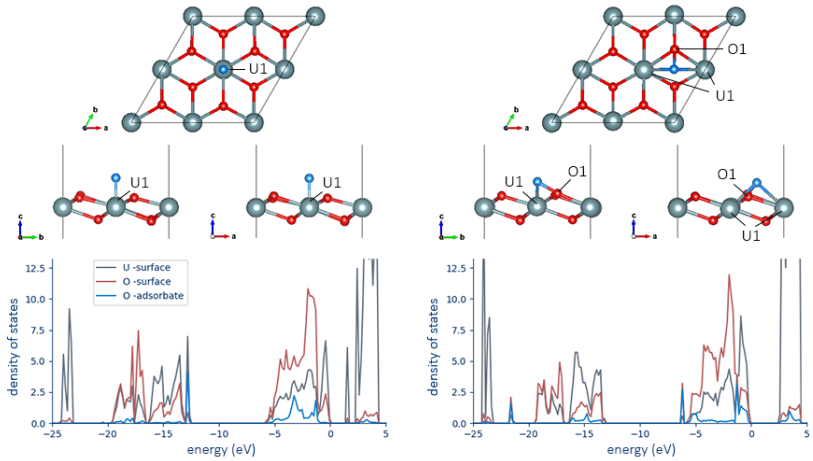

(a) (111) U-site chemisorption (b) (111) O-site chemisorption

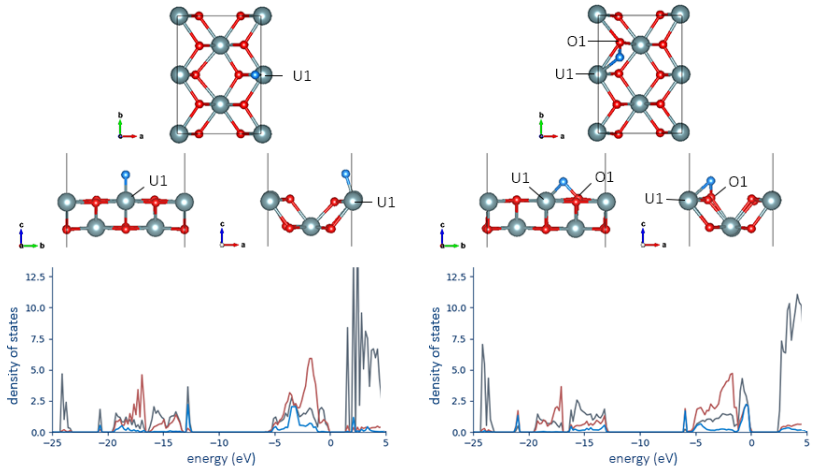

(c) (110) U-site chemisorption (d) (110) O-site chemisorption

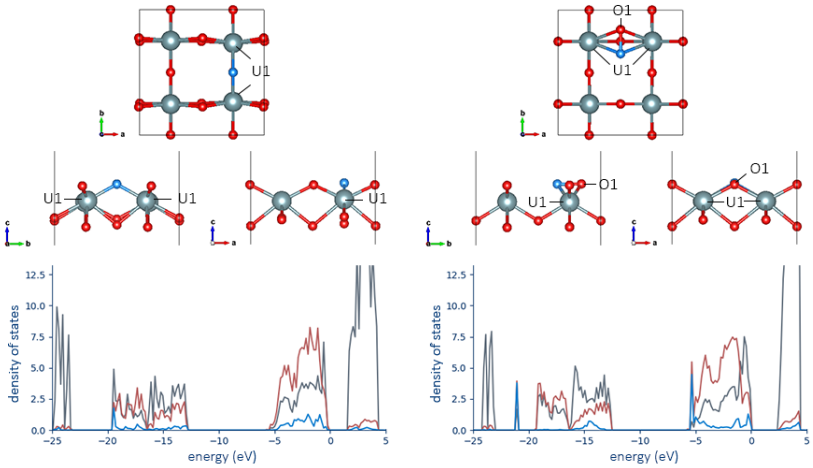

(e) (100) U-site chemisorption (f) (100) O-site chemisorption

Figure 5: Final atomic configurations and DOS for adsorption of the oxygen radical on three UO_2 surface models. The DOS shows only the contributions of the surface atoms: uranium in grey, oxygen in red and adsorbed oxygen in blue.

configuration	|OO| (Å)	|O_2surface| (Å)	|OU_1| (Å)	E_{ads} (eV)	e^- transfer
(111) surface					
physisorption (6a)	1.25	2.06	2.77	-0.24	/
(110) surface					
chemisorption (6c)	1.33	2.25	2.35	-1.05	0.57
physisorption (6b)	1.24	2.29	3.60	-0.19	/
(100) surface					
chemisorption (6e)	1.33	0.57	2.38, 2.44, 2.48	-0.52	0.64
physisorption (6d)	1.23	2.57	3.60	-0.05	/

Table 4: Summary of the adsorption of the oxygen molecule. In the first column the final configurations is described, followed by the relevant bond lengths, adsorption energies and Bader charge transfer from the surface to the adsorbate. O_2 and U_1 are labeled in Figure 6.

now occupying the anti-bonding orbital which facilitates dissociation. The O-U distance is similar to the O-U bond length in bulk UO_2. Again the U coordination is increased from 6 to 8. The molecule has a low spin state of 0.8 μ_B (Table S8 in SI). The U atom spin is decreased from 1.67 to 0.88 and 0.75 μ_B for the (110) and (100) respectively, which indicates an oxidation state of +V for the U atom. Unlike in the physisorbed case, in the DOS hybridization of adsorbates' states (s-states at -15 eV and p-states at -2 eV) with surface states is visible, as shown in Fig. 6c and 6e.
We also estimated the dissociation barrier of O_2 when chemisorbed to the surface. Starting from the case where oxygen is chemisorbed to the (110) surface (Fig. 6c), the bond length was increased by moving one of the oxygen atoms along the b direction (illustrated in Fig. S2 in the supporting information), until it was bound to the other uranium atom, like the case of adsorption of a single oxygen atom, Fig. 5c. This dissociation barrier is 2.88 eV for O_2 bound to the surface, compared to 6.04 eV for the isolated molecule. It is, however, very important to note that this result is only an upper bound to the dissociation energy of oxygen adsorbed to the surface, because a full Nudged Elastic Band (NEB) calculation was not feasible.

3.3.3. H_2O adsorption

On the two most stable surfaces ((111) and (110)) the only configuration for water adsorption is found to be chemisorption, with an adsorption energy of -0.73 eV and -0.94 eV, respectively, see Table 5. The O-U distance is 2.6 Å, the sum of the covalent radii for U and O. Bader analysis shows no charge transfer (Table S9 in SI), but hybridization of some oxygen states with the surface is seen in the DOS (Fig. 7a and 7b) around -4 eV between the oxygen p-states of the adsorbate and the surface.
On the (100)-surface two chemisorbed cases are found (Table 5). The energetically favored one is the dissociation molecule, Fig. 7c. Here two hydroxyl groups are formed on the surface: one of the hydrogen atoms is split from the molecule and binds with a surface oxygen atom. The remaining OH then binds to a uranium atom, increasing its coordination from 6 to 7, with a U-O bond length of 2.35 Å, which is similar to UO_2 bulk. The first hydroxyl gives rise to a sharp peak in the DOS (Fig. 7c) at -6.5 eV, consisting of contributions from the hydrogen atom and the oxygen of the surface, while the second one has a sharp peak

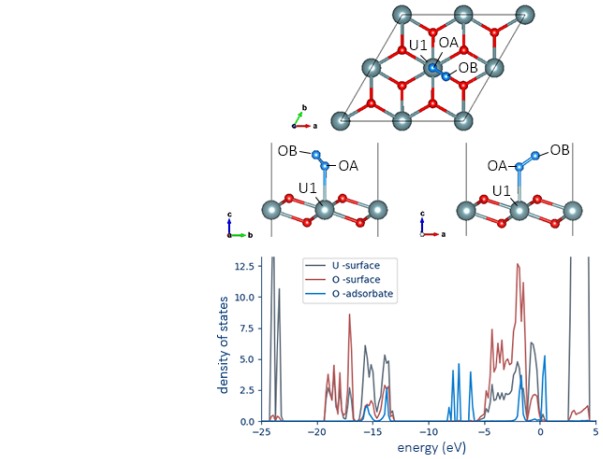

(a) (111) physisorption

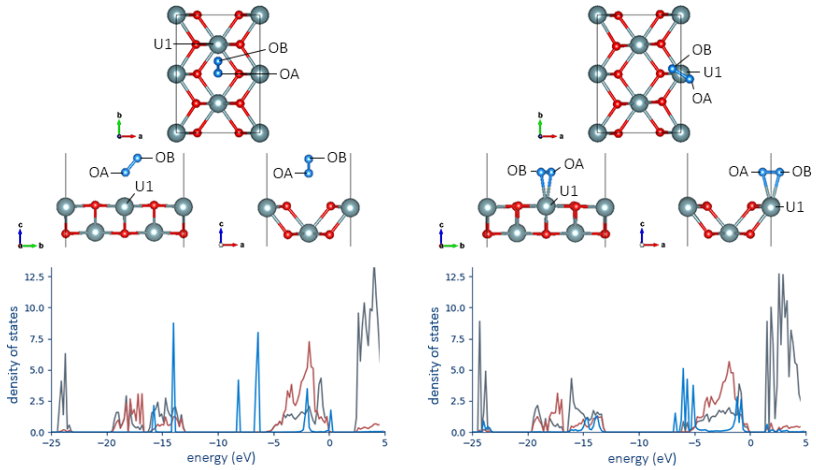

(b) (110) physisorption

(c) (110) chemisorption

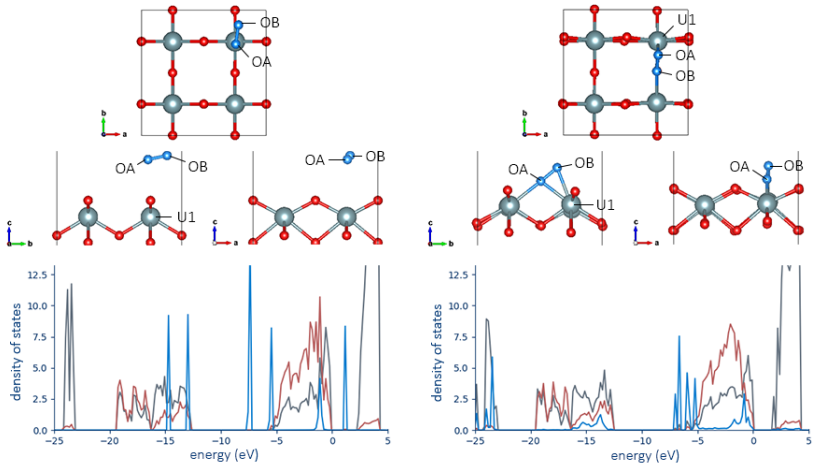

(d) (100) physisorption

(e) (100) chemisorption

Figure 6: Final atomic configurations and DOS for adsorption of the oxygen molecule on three UO_2 surface models. The DOS shows only the contributions of the surface atoms: uranium in grey, oxygen in red and adsorbed oxygen in blue.

configuration	|OH| (Å)	|O_1H| (Å)	|OU_1| (Å)	E_{ads} (eV)	E_{ads} literature	e^- transfer
(111) surface						
chemisorption (7a)	0.97, 1.01	1.69	2.60	-0.73	-0.61[a] -0.52[b] -0.53[c]	/
(110) surface						
chemisorption (7b)	0.99	2.16	2.66	-0.94	-0.62[a] -1.06[b] -0.93[c]	/
(100) surface						
dissociated (7c)	2.63, 0.97	0.97	2.35, 2.39	-1.90	-1.71[a] -1.55[c]	-0.34
chemisorption (7d)	0.98	2.63	2.65	-1.52	-1.02[a] -0.97[c]	/

Table 5: Summary of the adsorption of the water molecule. In the first column the final configurations is described, followed by the relevant bond lengths, adsorption energies and Bader charge transfer from the surface to the adsorbate. O_1 and U_1 are labeled in Figure 7. The literature values are by: [a] Bo et al. [8], [b] Wellington et al. [65], [c] Tegner et al. [60]

at -6 eV. Broadening of the oxygen states of the adsorbate at -19 eV (*s*-states) and -2 eV (*p*-states) is due to hybridization with the surface.
The other chemisorbed case on the (100)-surface is molecular adsorption (Fig. 7d), which is equivalent to the one found on the other two surfaces. No significant change in spin moment in any of these H_2O adsorption cases was observed, so the oxidation state of the U atoms remains +IV.

3.3.4. H_2O_2 adsorption

On all three surfaces a molecular adsorption has been found for H_2O_2, see Table 6, Fig. 8b, 8c and 8d. One of the oxygen atoms is bonded to a uranium atom, with a bond length of 2.6 Å (8 % larger than bulk UO_2). The OH bond lengths are unchanged (1 Å). The hydrogen atoms are oriented towards the surface and form hydrogen bridges with the surface oxygen atoms (O-H = 1.7 Å). The DOS shows again hybridization of *s*-states of the adsorbate at -18 eV and *p*-states in the valence band around -3 eV with the surface states, Fig 8b, 8c and 8d. No significant change in spin moment in any of the H_2O_2 adsorption cases was observed, so the oxidation state of the U atoms remains +IV.
On the (111)-surface a dissociated configuration (H + HO_2) is also found, see Table 6, Fig. 8a. Its adsorption energy is similar to the molecular case (-0.90 eV). The O-U distance is 2.35 Å, similar to bulk UO_2. One of the hydrogen atoms is split from the molecule and forms hydroxyl with a surface oxygen (1.0 Å), while it forms a hydrogen bond with the adsorbate. The hydrogen on the remaining adsorbate is directed away from the surface now. Electrons are transferred from the adsorbate to the surface (Table S10 in SI). The DOS offers a similar insight (Fig. 8a) as the molecular adsorption with the broadening of the adsorbates' states at -1, -4 and -17 eV. Of the sharp peaks between -5 and -10 eV one (at -7.5 eV) consists solely of states of the adsorbate, while the one at -6.5 eV indicates the hydroxyl bond between one hydrogen of the adsorbate and the surface oxygen.

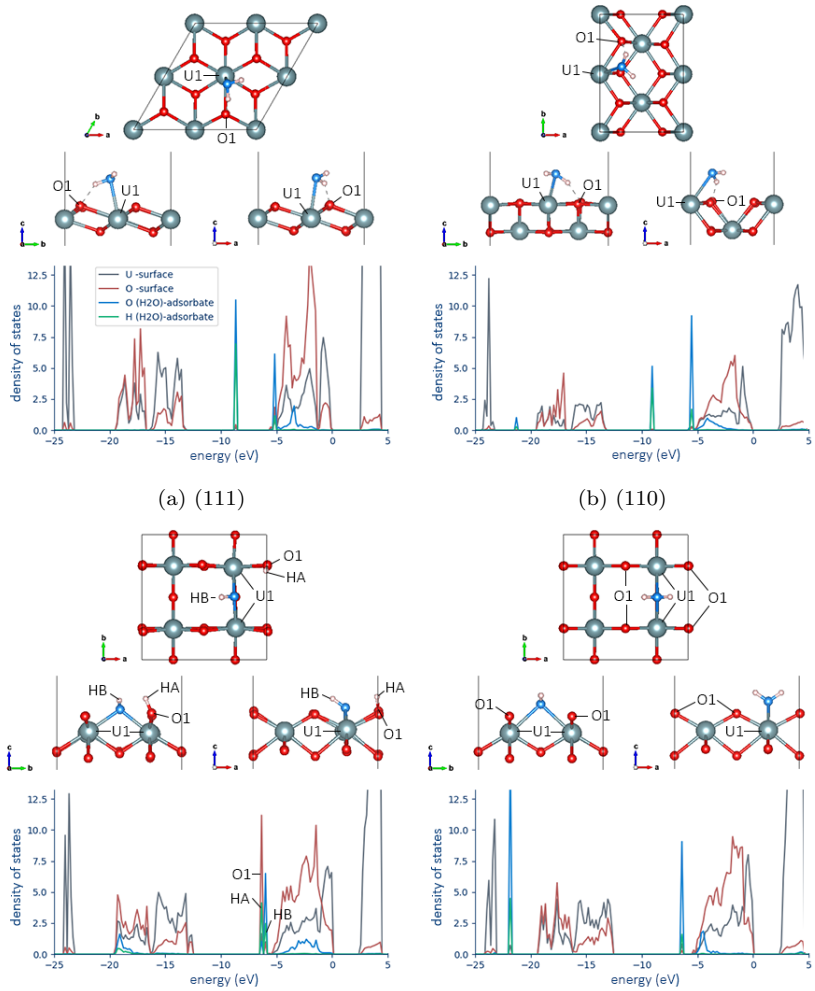

(a) (111)

(b) (110)

(c) (100) dissociated

(d) (100) molecular

Figure 7: Final atomic configurations and DOS for adsorption of the water molecule on three UO_2 surface models. The DOS shows only the contributions of the surface atoms: uranium in grey, oxygen in red, adsorbed oxygen in blue and hydrogen in green.

configuration	**|OH| (Å)**	**|O_1H| (Å)**	**|OO| (Å)**	**|OU_1| (Å)**	**E_{ads} (eV)**	**e^- transfer**
(111) surface						
molecular (8b)	0.99, 1.01	1.68, 1.95	1.47	2.61	-0.95	/
dissociated (8a)	0.98, 1.65	1.01	1.49	2.37	-0.90	-0.37
(110) surface						
chemisorption (8c)	1.02	1.61, 1.73	1.48	2.74	-1.38	/
(100) surface						
chemisorption (8d)	1.02	1.68, 1.77	1.47	2.64, 2.66	-1.34	/

Table 6: Summary of the adsorption of the hydrogen peroxide molecule. In the first column the final configurations is described, followed by the relevant bond lengths, adsorption energies and Bader charge transfer from the surface to the adsorbate. O_1 and U_1 are labeled in Figure 8.

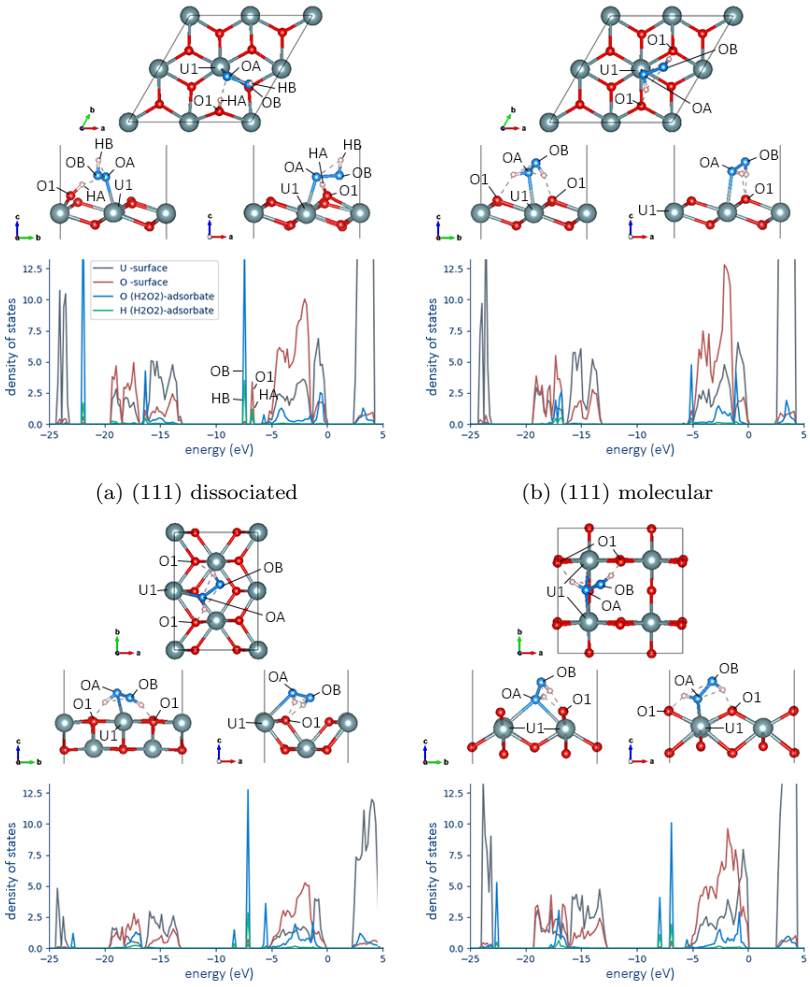

(a) (111) dissociated

(b) (111) molecular

(c) (110)

(d) (100)

Figure 8: Final atomic configurations and DOS for adsorption of the hydrogen peroxide molecule on three UO_2 surface models. The DOS shows only the contributions of the surface atoms: uranium in grey, oxygen in red, adsorbed oxygen in blue and hydrogen in green.

4. Discussion

4.1. Bulk and pristine surface

Results on UO_2 bulk and surface were presented in order to validate the computational approach. Though two comments can be made regarding these results. Firstly, the calculated oxygen displacement in bulk is 0.0043 Å, a factor 3 smaller than measured with neutron diffraction (0.014 Å) [19], while other *ab initio* studies using the $3k$ transverse order consistently find larger values: 0.034 Å (HSE06 with SOC) [47], 0.09 Å (PBE+U without SOC) [21] and 0.075 Å (LDA+U with SOC, all electron) [32]. This deviation on the small oxygen displacement does not affect the results presented in this work. The most important aspect is the use of non-collinear $3k$ transverse magnetism to retain the cubic structure of UO_2 (collinear AFM leads to tetragonal symmetry) and inclusion of SOC to qualitatively reproduce the Jahn-Teller distortion.

Secondly, in all surface models, the direction of the magnetic moments in the center layers does not converge to bulk order. This discrepancy could be attributed to several factors: the near-degeneracy of the magnetic orders, the possibility that the surface model slab size is not large enough compared to the magnetic correlation length, or it may result from frustration of the magnetic moments due to the symmetry of the slab model. However, other properties such as the magnitude of the magnetic moments and Bader charge (both can be found in Fig. S1 in the supporting information), as well as the electronic structure, do converge to bulk values. Since the focus of the study is on investigating surface properties, this is not expected to significantly influence the results.

4.2. Adsorption

For each adsorbate studied, the adsorption on the (111) surface is least favored, because of the higher adsorption energy. Adsorption to the (110) surface is favored for adsorbates that feature an O-O bond (O_2 and H_2O_2), while (100) is favored for O and H_2O. This is due to the geometry of the surface, because in the (100) surface model two uranium atoms are involved in the adsorption.

Investigation of the uranium spin magnetic moment at the surface, allows us to categorize the uranium oxidation state [33]. The surface uranium atoms are oxidized to a +V or +VI state because of the adsorption of the oxygen radical to a uranium atom and the chemisorption of the O_2 molecule. Dissociative water and hydrogen peroxide adsorption do not lead to a change of oxidation state, despite the increase in uranium coordination. The electron transfer to the surface is localized on the surface oxygen.

Adsorption of molecular O_2 to the (111) surface only results in a physisorbed state, in contrast with the other two surfaces. This despite the initial distance to the surface of only 1 Å to stimulate the system into formation of a bond. It is unlikely that the stoichiometric (111) surface will play a role in dissociation of O_2.

Upon comparing the final positions and bond lengths of water adsorption with previous work [8, 65, 60] (Table 5), we note their similarity, indicating no discernible influence of spin-orbit coupling and non-collinear effects. The present study calculated lower adsorption energies for the (100) and (111) surfaces compared to earlier work. For (111) surfaces, a broad range of adsorption energies was reported, and our calculations are within the earlier reported range. Interestingly, the dissociation reaction ($H_2O \rightarrow H + OH$) was in our study only found for (100) surfaces, but not for (111) and (110). Other studies [8, 60] reported that the dissociated configuration has a lower energy on all three surfaces. Wellington et al. [65] only studied (111) and (110), and also found lower energies for the dissociated configuration. Although the energy barrier of the dissociation reaction was not explicitly calculated in our study, it likely prohibits formation of of the dissociated state on the (111) and (110) surfaces starting from an intact molecule.

In [44], hydrogen adsorption on the (111) UO_2 surface is studied. When a hydroxyl group is formed, reduction of a uranium atom away from the OH group and a U-f defect state in the band gap were found. It was argued that this was most likely a limitation of the size of the supercell. In the present study, we did, however, not observe the reduction of U away from the hydroxyl group when it is formed after adsorption of H_2O_2 on the (111) surface, nor after adsorption of H_2O on the (100) surface. This is probably due to the adsorption of the residual molecule over which the charge can be distributed.

In future work, it is recommended to explore co-adsorption of the molecules studied here, specifically examining the influence of hydroxyl groups to O_2 adsorption, as the hydroxyl groups potentially lead to increased reactivity due to the reduction of the surface. Further extending to reduced surfaces with oxygen vacancies, to study dissociation pathways and the penetration of oxygen into different layers. It's important to note that performing non-collinear NEB calculations remain practically impossible due to the computational cost.

5. Conclusions

In the context of oxidation of uranium dioxide, adsorption on UO_2 surfaces has been studied in order to model the initial phase of the oxidation where oxygen or water molecules are first chemisorbed to the surface. The models include SOC and non-collinear $3k$ AFM magnetization in order to calculate accurate structures and energies. The interactions of atomic O, O_2, H_2O and H_2O_2 with the UO_2 surfaces ((111), (110) and (100)) have been investigated. Due to the inclusion of spin orbit coupling, the model of uranium dioxide is more accurate than previous studies. This work establishes the results of previous studies on water adsorption with higher confidence. The adsorption energies for water were previously underestimated, but the adsorption configurations, including bond lengths and their relative stability, are confirmed. The magnetic moments at the surface layer are realigned towards the surface plane, in contrast with the situation in bulk.

Generally, adsorption to the (111) surface, which is the most stable free surface, is less

preferred due to the higher adsorption energy. At low temperature (where water was found to be more strongly oxidizing [14]), the oxygen molecule will be stuck in a physisorbed state, which does not oxidize the surface. The chemisorption energies of water compared to oxygen is lower for the (100), but not for the (110) surface. The most favoured adsorption position for each case always features a bond of an oxygen atom with a surface uranium atom. Whether adsorption is favoured on the (110) or (100) surface depends on the presence of an O-O bond in the adsorbate; it tries to attain the ideal uranium coordination, which is affected by the geometry of the surface.

On the (110) and (100) chemisorption is found for O_2, where the oxidation state of the involved uranium atom is increased to +V, indicated by a decrease of the U spin. Superoxide is formed according to the O-O bond length and confirmed by Bader charges, which lowers the oxygen dissociation energy. The dissociation barrier is estimated to be 2.88 eV, compared to 6.04 eV for isolated O_2. For H_2O, dissociation is found on the (100) surface, leading to the formation of two hydroxyl groups and a reduction of the surface, though the oxidation state of the surface U atoms remains +IV. The adsorption energy of H_2O_2 on the (111) and (110) is lower than that of water. Moreover, on the (111) surface, the H_2O_2 molecule may dissociate into a hydrogen radical and a hydroperoxyl radical. The hydrogen radical reacts with a surface oxygen to form a hydroxyl group, leading to the reduction of that surface oxygen atom.

Acknowledgments

Financial support for this research was provided by the Energy Transition Fund of the Belgian FPS Economy (Project SF-CORMOD: Spent Fuel - Corrosion modeling). This work was performed using HPC resources from the VSC (Flemish Supercomputer Center) and the HPC infrastructure of the University of Antwerp (CalcUA), both funded by the FWO-Vlaanderen and the Flemish Government department EWI (Economie, Wetenschap & Innovatie).

References

[1] Allen, G.C., Tempest, P.A., 1982. Linear ordering of oxygen clusters in hyperstoicheiometric uranium dioxide. J. Chem. Soc., Dalton Trans. 1982, 2169–2173. doi:10.1039/DT9820002169.

[2] Allen, G.C., Tempest, P.A., 1983. The accommodation of oxygen clusters in hyperstoicheiometric uranium dioxide and its effects on crystal structure. J. Chem. Soc., Dalton Trans. 1983, 2673–2677. doi:10.1039/DT9830002673.

[3] Amadon, B., Applencourt, T., Bruneval, F., 2014. Screened Coulomb interaction calculations: cRPA implementation and applications to dynamical screening and self-consistency in uranium dioxide and cerium. Phys. Rev. B 89, 125110. doi:10.1103/PhysRevB.89.125110.

[4] Andersson, D.A., Baldinozzi, G., Desgranges, L., Conradson, D.R., Conradson, S.D., . Density functional theory calculations of UO2 oxidation: Evolution of UO2+x, u4o9–y, u3o7, and u3o8. Inorg. Chem. 52, 2769–2778. doi:10.1021/ic400118p. publisher: American Chemical Society.

[5] Ao, B., Qiu, R., Lu, H., Chen, P., 2016. Differences in the Existence States of Hydrogen in UO_2 and PuO_2 from DFT + U Calculations. J. Phys. Chem. C 120, 18445–18451. doi:10.1021/acs.jpcc.6b05621.

[6] Baer, Y., Schoenes, J., 1980. Electronic structure and Coulomb correlation energy in UO2 single crystal. Solid State Communications 33, 885–888. doi:10.1016/0038-1098(80)91210-7.
[7] Blackburn, P.E., Weissbart, J., Gulbransen, E.A., 1958. Oxidation of Uranium Dioxide. J. Phys. Chem. 62, 902–908. doi:10.1021/j150566a002.
[8] Bo, T., Lan, J.H., Wang, C.Z., Zhao, Y.L., He, C.H., Zhang, Y.J., Chai, Z.F., Shi, W.Q., 2014a. First-Principles Study of Water Reaction and H_2 Formation on UO_2 (111) and (110) Single Crystal Surfaces. J. Phys. Chem. C 118, 21935–21944. doi:10.1021/jp503614f.
[9] Bo, T., Lan, J.H., Zhao, Y.L., Zhang, Y.J., He, C.H., Chai, Z.F., Shi, W.Q., 2014b. First-principles study of water adsorption and dissociation on the UO_2 (111), (110) and (100) surfaces. Journal of Nuclear Materials 454, 446–454. doi:10.1016/j.jnucmat.2014.09.001.
[10] Bryenton, K.R., Adeleke, A.A., Dale, S.G., Johnson, E.R., 2023. Delocalization error: The greatest outstanding challenge in density-functional theory. Wiley Interdiscip. Rev.-Comput. Mol. Sci. 13, e1631. doi:10.1002/wcms.1631.
[11] Cabrera, N., Mott, N.F., 1949. Theory of the oxidation of metals. Rep. Prog. Phys. 12, 163. doi:10.1088/0034-4885/12/1/308.
[12] Ditter, A.S., Pacold, J.I., Dai, Z., Lee Davisson, M., Vine, D., Donald, S.B., Chung, B.W., Shuh, D.K., 2022. Submicrometer spectromicroscopy of UO_2 aged under high humidity conditions. Journal of Vacuum Science & Technology A 40, 043202. doi:10.1116/6.0001880.
[13] Donald, S.B., Dai, Z.R., Davisson, M.L., Jeffries, J.R., Nelson, A.J., 2017a. An XPS study on the impact of relative humidity on the aging of UO_2 powders. Journal of Nuclear Materials 487, 105–112. doi:10.1016/j.jnucmat.2017.02.016.
[14] Donald, S.B., Davisson, M.L., Dai, Z., Roberts, S.K., Nelson, A.J., 2017b. Relative impact of H_2O and O_2 in the oxidation of UO_2 powders from 50 to 300 °C. Journal of Nuclear Materials 496, 353–361. doi:10.1016/j.jnucmat.2017.10.014.
[15] Dorado, B., Amadon, B., Freyss, M., Bertolus, M., 2009. DFT+U calculations of the ground state and metastable states of uranium dioxide. Physical Review B 79, 235125. doi:10.1103/PhysRevB.79.235125.
[16] Dorado, B., Freyss, M., Amadon, B., Bertolus, M., Jomard, G., Garcia, P., 2013. Advances in first-principles modelling of point defects in UO_2: f electron correlations and the issue of local energy minima. J. Phys.-Condes. Matter 25, 333201. doi:10.1088/0953-8984/25/33/333201.
[17] Dudarev, S.L., Botton, G.A., Savrasov, S.Y., Humphreys, C.J., Sutton, A.P., 1998. Electron-energy-loss spectra and the structural stability of nickel oxide: An LSDA+U study. Phys. Rev. B 57, 1505–1509. doi:10.1103/PhysRevB.57.1505.
[18] Faber, J., Lander, G.H., 1976. Neutron diffraction study of UO_2: Antiferromagnetic state. Phys. Rev. B 14, 1151–1164. doi:10.1103/PhysRevB.14.1151.
[19] Faber, J., Lander, G.H., Cooper, B.R., 1975. Neutron-Diffraction Study of UO_2: Observation of an Internal Distortion. Phys. Rev. Lett. 35, 1770–1773. doi:10.1103/PhysRevLett.35.1770.
[20] Ferguson, I., Mcconnell, J., 1957. Heat of Adsorption of Oxygen on Uranium Dioxide at -183°C. Proc. R. Soc. Lond. A 241, 67–79. doi:10.1098/rspa.1957.0113.
[21] Freyss, M., Dorado, B., Bertolus, M., Jomard, G., Vathonne, E., Garcia, P., Amadon, B., 2012. First-principles DFT+U study of radiation damage in UO_2: f electron correlations and the local energy minima issue. Ψ_k Scientific Highlight Of The Month October 2012, No. 113.
[22] Fromhold, A., 1980. Theory of Metal Oxidation. Number v. 2 in Defects in crystalline solids, North-Holland.
[23] Grambow, B., 2021. Spent nuclear fuel long term behavior and performance, in: Greenspan, E. (Ed.), Encyclopedia of Nuclear Energy. Elsevier, Oxford, pp. 577–587. doi:10.1016/B978-0-12-819725-7.00155-0.
[24] Grimme, S., 2006. Semiempirical GGA-type density functional constructed with a long-range dispersion correction. Journal of Computational Chemistry 27, 1787–1799. doi:10.1002/jcc.20495.
[25] Henkelman, G., Arnaldsson, A., Jónsson, H., 2006. A fast and robust algorithm for Bader decomposition of charge density. Computational Materials Science 36, 354–360. doi:10.1016/j.commatsci.2005.04.010.
[26] Kotani, A., Yamazaki, T., 1992. Systematic Analysis of Core Photoemission Spectra for Actinide

Di-Oxides and Rare-Earth Sesqui-Oxides. Progress of Theoretical Physics Supplement 108, 117–131. doi:10.1143/PTPS.108.117.

[27] Kresse, G., Furthmüller, J., 1996. Efficient iterative schemes for ab initio total-energy calculations using a plane-wave basis set. Phys. Rev. B 54, 11169–11186. doi:10.1103/PhysRevB.54.11169.

[28] Kresse, G., Joubert, D., 1999. From ultrasoft pseudopotentials to the projector augmented-wave method. Phys. Rev. B 59, 1758–1775. doi:10.1103/PhysRevB.59.1758.

[29] Kursten, B., Druyts, F., 2008. Methodology to make a robust estimation of the carbon steel overpack lifetime with respect to the Belgian Supercontainer design. Journal of Nuclear Materials 379, 91–96. doi:10.1016/j.jnucmat.2008.06.020.

[30] Kursten, B., Druyts, F., Macdonald, D.D., Smart, N.R., Gens, R., Wang, L., Weetjens, E., Govaerts, J., 2011. Review of corrosion studies of metallic barrier in geological disposal conditions with respect to Belgian Supercontainer concept. Corrosion Engineering, Science and Technology 46, 91–97. doi:10.1179/1743278210Y.0000000022.

[31] Labroche, D., Dugne, O., Chatillon, C., 2003. Thermodynamic properties of the O–U system. II – Critical assessment of the stability and composition range of the oxides UO_{2+x}, U_4O_{9-y} and U_3O_{8-z}. Journal of Nuclear Materials 312, 50–66. doi:10.1016/S0022-3115(02)01323-5.

[32] Laskowski, R., Madsen, G.K.H., Blaha, P., Schwarz, K., 2004. Magnetic structure and electric-field gradients of uranium dioxide: An ab initio study. Phys. Rev. B 69, 140408. doi:10.1103/PhysRevB.69.140408.

[33] Leinders, G., Baldinozzi, G., Ritter, C., Saniz, R., Arts, I., Lamoen, D., Verwerft, M., 2021. Charge Localization and Magnetic Correlations in the Refined Structure of U_3O_7. Inorg. Chem. 60, 10550–10564. doi:10.1021/acs.inorgchem.1c01212.

[34] Leinders, G., Cardinaels, T., Binnemans, K., Verwerft, M., 2015. Accurate lattice parameter measurements of stoichiometric uranium dioxide. Journal of Nuclear Materials 459, 135–142. doi:10.1016/j.jnucmat.2015.01.029.

[35] Leinders, G., Cardinaels, T., Binnemans, K., Verwerft, M., 2018. Low-Temperature Oxidation of Fine UO_2 Powders: Thermochemistry and Kinetics. Inorg. Chem. 57, 4196–4204. doi:10.1021/acs.inorgchem.8b00517.

[36] Lemmens, K., González-Robles, E., Kienzler, B., Curti, E., Serrano-Purroy, D., Sureda, R., Martínez-Torrents, A., Roth, O., Slonszki, E., Mennecart, T., Günther-Leopold, I., Hózer, Z., 2017. Instant release of fission products in leaching experiments with high burn-up nuclear fuels in the framework of the Euratom project FIRST- Nuclides. Journal of Nuclear Materials 484, 307–323. doi:10.1016/j.jnucmat.2016.10.048.

[37] Maldonado, P., Evins, L.Z., Oppeneer, P.M., 2014. Ab Initio Atomistic Thermodynamics of Water Reacting with Uranium Dioxide Surfaces. J. Phys. Chem. C 118, 8491–8500. doi:10.1021/jp501715m.

[38] McEachern, R.J., Taylor, P., 1998. A review of the oxidation of uranium dioxide at temperatures below 400°C. Journal of Nuclear Materials 254, 87–121. doi:10.1016/S0022-3115(97)00343-7.

[39] Meek, T.T., von Roedern, B., Clem, P.G., Hanrahan, R.J., 2005. Some optical properties of intrinsic and doped UO_2 thin films. Materials Letters 59, 1085–1088. doi:10.1016/j.matlet.2004.12.012.

[40] Mennecart, T., Iglesias, L., Herm, M., König, T., Leinders, G., Cachoir, C., Lemmens, K., Verwerft, M., Metz, V., González-Robles, E., Meert, K., Vandoorne, T., Gaggiano, R., 2024. Effect of hydrogen gas and leaching solution on the fast release of fission products from two PWR fuels. Journal of Nuclear Materials 588, 154811. doi:10.1016/j.jnucmat.2023.154811.

[41] Middleburgh, S.C., Dumbill, S., Qaisar, A., Vatter, I., Owen, M., Vallely, S., Goddard, D., Eaves, D., Puide, M., Limbäck, M., Lee, W.E., 2023. Enrichment of Chromium at Grain Boundaries in Chromia Doped UO_2. Journal of Nuclear Materials 575, 154250. doi:10.1016/j.jnucmat.2023.154250.

[42] Muggelberg, C., Castell, M.R., Briggs, G.A.D., Goddard, D.T., 1999. An STM study of the UO2(001) surface. Applied Surface Science 142, 124–128. doi:10.1016/S0169-4332(98)00664-3.

[43] Pegg, J.T., Aparicio-Anglès, X., Storr, M., de Leeuw, N.H., 2017. DFT+U study of the structures and properties of the actinide dioxides. Journal of Nuclear Materials 492, 269–278. doi:10.1016/j.jnucmat.2017.05.025.

[44] Pegg, J.T., Shields, A.E., Storr, M.T., Scanlon, D.O., de Leeuw, N.H., 2019a. Interaction of hydrogen with actinide dioxide (111) surfaces. The Journal of Chemical Physics 150, 134701. doi:10.1063/1.5087577.

[45] Pegg, J.T., Shields, A.E., Storr, M.T., Scanlon, D.O., de Leeuw, N.H., 2019b. Noncollinear Relativistic DFT + U Calculations of Actinide Dioxide Surfaces. J. Phys. Chem. C 123, 356–366. doi:10.1021/acs.jpcc.8b07823.

[46] Pegg, J.T., Shields, A.E., Storr, M.T., Scanlon, D.O., de Leeuw, N.H., 2020. Interaction of hydrogen with actinide dioxide (011) surfaces. The Journal of Chemical Physics 153, 014705. doi:10.1063/5.0010200.

[47] Pegg, J.T., Shields, A.E., Storr, M.T., Wills, A.S., Scanlon, D.O., de Leeuw, N.H., 2019c. Magnetic structure of UO_2 and NpO_2 by first-principle methods. Phys. Chem. Chem. Phys. 21, 760–771. doi:10.1039/C8CP03581D.

[48] Perdew, J.P., Burke, K., Ernzerhof, M., 1996. Generalized Gradient Approximation Made Simple. Phys. Rev. Lett. 77, 3865–3868. doi:10.1103/PhysRevLett.77.3865.

[49] Poinssot, C., Ferry, C., Lovera, P., Jegou, C., Gras, J.M., 2005. Spent fuel radionuclide source term model for assessing spent fuel performance in geological disposal. Part II: Matrix alteration model and global performance. Journal of Nuclear Materials 346, 66–77. doi:10.1016/j.jnucmat.2005.05.021.

[50] Rák, Zs., Ewing, R., Becker, U., 2013. Hydroxylation-induced surface stability of AnO_2 (An=U, Np, Pu) from first-principles. Surface Science 608, 180–187. doi:10.1016/j.susc.2012.10.002.

[51] Roberts, L.E.J., 1954. The oxides of uranium. Part V. The chemisorption of oxygen on UO $_2$ and on U_2O –ThO_2 solid solutions. J. Chem. Soc. 0, 3332–3339. doi:10.1039/JR9540003332.

[52] Saniz, R., Baldinozzi, G., Arts, I., Lamoen, D., Leinders, G., Verwerft, M., 2023. Charge order, frustration relief, and spin-orbit coupling in U_3O_8. Phys. Rev. Mater. 7, 054410. doi:10.1103/PhysRevMaterials.7.054410.

[53] Schoenes, J., 1978. Optical properties and electronic structure of UO_2. Journal of Applied Physics 49, 1463–1465. doi:10.1063/1.324978.

[54] Schoenes, J., 1987. Recent spectroscopic studies of UO_2. J. Chem. Soc., Faraday Trans. 2 83, 1205–1213. doi:10.1039/F29878301205.

[55] Schreinemachers, C., Leinders, G., Mennecart, T., Cachoir, C., Lemmens, K., Verwerft, M., Brandt, F., Deissmann, G., Modolo, G., Bosbach, D., 2022. Caesium and iodine release from spent mixed oxide fuels under repository relevant conditions: Initial leaching results. MRS Advances 7, 100–104. doi:10.1557/s43580-022-00220-7.

[56] Sholl, D.S., Steckel, J.A., 2009. DFT Calculations for Surfaces of Solids, in: Density Functional Theory. John Wiley & Sons, Ltd. chapter 4, pp. 83–112. doi:10.1002/9780470447710.ch4.

[57] Suzuki, M.T., Magnani, N., Oppeneer, P.M., 2013. Microscopic theory of the insulating electronic ground states of the actinide dioxides AnO_2(An = U, Np, Pu, Am, and Cm). Phys. Rev. B 88, 195146. doi:10.1103/PhysRevB.88.195146.

[58] Taylor, P., Burgess, E.A., Owen, D.G., 1980. An X-ray diffraction study of the formation of β-UO_2.33 on UO_2 pellet surfaces in air at 229 to 275°C. Journal of Nuclear Materials 88, 153–160. doi:10.1016/0022-3115(80)90395-5.

[59] Tegner, B.E., Kaltsoyannis, N., 2018. Multiple water layers on AnO_2 {111}, {110}, and {100} surfaces (An = U, Pu): A computational study. Journal of Vacuum Science & Technology A 36, 041402. doi:10.1116/1.5028210.

[60] Tegner, B.E., Molinari, M., Kerridge, A., Parker, S.C., Kaltsoyannis, N., 2017. Water Adsorption on AnO_2 {111}, {110}, and {100} Surfaces (An = U and Pu): A Density Functional Theory + U Study. J. Phys. Chem. C 121, 1675–1682. doi:10.1021/acs.jpcc.6b10986.

[61] Tian, X.f., Wang, H., Xiao, H.x., Gao, T., 2014. Adsorption of water on UO_2 (111) surface: Density functional theory calculations. Computational Materials Science 91, 364–371. doi:10.1016/j.commatsci.2014.05.009.

[62] Tiferet, E., Mintz, M.H., Jacob, I., Shamir, N., 2007. Inhibition of hydrogen chemisorption on uranium surfaces by traces of water vapor. Surface Science 601, 4925–4930. doi:10.1016/j.susc.2007.08.005.

[63] Van Geet, M., Weetjens, E., 2009. Strategic Choices in the Belgian Supercontainer Design and Its Treatment in a Safety Case. Technical Report. Nuclear Energy Agency of the OECD (NEA). Brussels.
[64] Wang, G., Batista, E.R., Yang, P., 2020. Water on Actinide Dioxide Surfaces: A Review of Recent Progress. Applied Sciences 10, 4655. doi:10.3390/app10134655.
[65] Wellington, J.P., Kerridge, A., Austin, J., Kaltsoyannis, N., 2016. Electronic structure of bulk AnO_2 (An = U, Np, Pu) and water adsorption on the (111) and (110) surfaces of UO_2 and PuO_2 from hybrid density functional theory within the periodic electrostatic embedded cluster method. Journal of Nuclear Materials 482, 124–134. doi:10.1016/j.jnucmat.2016.10.005.
[66] Wellington, J.P.W., Tegner, B.E., Collard, J., Kerridge, A., Kaltsoyannis, N., 2018. Oxygen Vacancy Formation and Water Adsorption on Reduced AnO_2{111}, {110}, and {100} Surfaces (An = U, Pu): A Computational Study. J. Phys. Chem. C 122, 7149–7165. doi:10.1021/acs.jpcc.7b11512.
[67] Yang, L., Wirth, B.D., . Clustering of excess oxygen in uranium dioxide: A first-principles study. Journal of Nuclear Materials 554, 153087. doi:10.1016/j.jnucmat.2021.153087.
[68] Yun, Y., Kim, H., Lim, H., Park, K., 2007. Electronic Structure of UO_2 from the Density Functional Theory with On-Site Coulomb Repulsion. Journal of the Korean Physical Society 50, 1285–1289. doi:10.3938/jkps.50.1285.